RESEARCH ARTICLE - APPLIED GEOPHYSICS



Simplified interpretation method by combining interval and direct methods for seismic downhole tests

Ayush Kumar¹ · P. Anbazhagan¹

Received: 6 November 2024 / Accepted: 12 April 2025 © The Author(s) under exclusive licence to Institute of Geophysics, Polish Academy of Sciences 2025

Abstract

Conventional downhole survey interpretation utilizes a straight raypath assumption from source to receiver, neglecting subsurface refractions along the travel path, which simplifies the estimation of shear wave velocity (V_S) profiles and average velocity (V_S) . Out of the most commonly used direct method (DM) and interval method (IM), IM is susceptible to sudden changes in subsurface stiffness due to high impedance contrast and anomalies, prompting the use of more detailed refracted raypath method (RRM) in such cases. However, RRM requires velocity of all the layers above the depth concerned. To avoid such dependency on the previous layers, a new interpretation approach combined direct interval method (CDIM) is proposed. The interfaces at impedance contrasts were observed to cause errors in V_S estimation while using IM. A parametric model study was conducted with varying depths and magnitude of impedance contrasts. Model study and downhole data acquired from five test sites showed that the errors associated with V_S estimation using CDIM are substantially lower than IM. The interval length for all the interpretation methods converges to the testing interval as the depth increases, which signifies that for greater depths and in the absence of high impedance contrasts in shallow depths, proposed CDIM offers a streamlined and fast interpretation, applicable for any geology and subsurface layering condition and can provide quick resolution of V_S profiles.

Keywords Shear wave velocity · Downhole test · Interval method · Direct method · Impedance contrast

Introduction

Small strain dynamic properties such as shear wave velocity (V_S) and in situ maximum shear modulus $(G_{\rm max})$ of the subsurface are essential in studying the influence of seismic and vibration load on the structures (Anomohanran 2013; Bajaj and Anbazhagan 2021, 2023; Bang et al. 2014; Boore et al. 2021; Boore and Thompson 2007; Brown et al. 2002; Koedel and Karl 2020; Kumar and Anbazhagan 2023). These properties can be determined using seismic geophysical methods or laboratory tests. Geophysical methods enable to determine the in situ properties and their spatial variation required for geotechnical design and modeling through an integrated approach (Anbazhagan 2018; Anbazhagan et al. 2022).

Edited by Prof. Dr. Liang Xiao (ASSOCIATE EDITOR) / Prof. Ali Gholami (CO-EDITOR-IN-CHIEF).

Published online: 28 May 2025

Among the geophysical methods, borehole and surface-based methods are the two categories of seismic tests (Brown et al. 2002; Darko et al. 2020; Garofalo et al. 2016a; b; Kim et al. 2013). Borehole-based methods directly measure the velocities of waves traveling from the source to the receiver. Among the borehole methods, the downhole survey is an important geophysical exploration method and is instrumental in determining subsurface dynamic properties and seismic site class. Being a borehole-based method, the downhole survey estimates wave velocities using the source-to-receiver distance and the arrival time of the wave to a receiver at the positioned depth (Bang et al. 2014; D7400-19 2019; Kim et al. 2004a; Stokoe et al. 2008). Additionally, samples during borehole drilling are collected and can be further assessed using laboratory investigations (Daraei et al. 2024). The test is easy to perform with a wooden beam and sledgehammer as source. In recent times, more extensive investigations have been carried out for critical infrastructure facilities such as oil wells and nuclear research laboratories (Daraei et al. 2024; Di Fiore et al. 2020; Naville et al. 2004; Stokoe et al. 2017; Vergniault and Mari 2020). Downhole surveys have been extensively used



 [□] P. Anbazhagan anbazhagan@iisc.ac.in

Indian Institute of Science, Bangalore, Karnataka, India

for site classification, deep velocity profiling and near-surface fault mapping in geotechnical earthquake engineering studies (Boore 2016; Boore and Asten 2008; Brown et al. 2002; Campbell and Boore 2016; Kumar and Anbazhagan 2023, 2025; Li 2008; Moffat et al. 2016; Stokoe et al. 2008, 2017; Wang et al. 2022). Besides the conventional uses, downhole survey has also been used for identification of weathered layer and sinkholes (Daraei et al. 2024) and stability analysis of reclaimed land (Wang et al. 2021a; b). These studies have contributed in development of test procedure and interpretation methods tailored to site-specific requirements (Boore and Thompson 2007; Di Fiore et al. 2020; Kumar and Anbazhagan 2023; Stokoe et al. 2017; Stolte and Cox 2020; Wang et al. 2021b). The improvement in downhole test procedures and interpretation methods assisted with easy workability has led to the widespread popularity of downhole tests (Anomohanran 2013; Bautista and Aguilar 2023a; Butcher et al. 2005; Kim et al. 2004b; Wang et al. 2021a).

Downhole test results are commonly used to determine average shear wave velocities for site classification (Boore and Thompson 2007; Kumar and Anbazhagan 2023). With the development of interpretation techniques, the test is now used for detailed V_S profiling with high resolution (Bang et al. 2014; Kim et al. 2004b). Among the several reduction methods available for downhole tests, the two most used ones are the direct method (DM) and the interval method (IM). These two methods are extensively used in the interpretation of the downhole tests. DM results in an average V_s profile between the two interface depths in the subsurface. This profile neglects any sudden changes or thin anomalies in the subsurface. A major concern with the use of the IM is that it does not consider the realistic time difference and length of travel path between two subsequent depths for the calculation of V_S . This problem often leads to negative or unexpectedly high V_S values in the presence of high V_S contrasts and thin subsurface V_S anomalies/layer (Hallal and Cox 2019; Kim et al. 2004b). Conversely, the direct method neglects the sudden or sharp changes in the V_s profile between two interfaces and results in an average $V_{\rm S}$ profile (Bautista and Aguilar 2023a; D7400-19 2019; Fernandez et al. 2008; Hallal and Cox 2019; Kim et al. 2004a; Kumar and Anbazhagan 2023). For higher accuracy and more realistic resolution of V_S profile, the refracted raypath method (RRM) is used in such critical scenarios (Bang et al. 2014; Boore and Thompson 2007; Kim et al. 2004a). However, RRM works only in order of increasing depth, i.e., first, the V_S of the shallower layer is calculated, followed by the deeper layer. Moreover, RRM requires an iterative procedure with boundary conditions, such as Snell's law to calculate V_S , and becomes computationally intensive. The V_S profiles obtained from these methods depend upon the sensitivity and robustness of the coded algorithm used during the inversion procedure. Any error induced in the V_S of a shallower

layer will be carried forward to the deeper layers. A simple method of interpretation, which is combined direct and interval method (CDIM) to remove the dependency on the upper layers for V_S estimation is proposed in this study. The efficacy of this method is studied using the two-layer subsurface model with varying magnitude and depth of V_S contrast, and further the V_S values obtained from field downhole surveys at five distinct locations using CDIM are compared with the RRM, IM and DM to assess its applicability in various lithological conditions. A major influencing factor on V_S calculation is the interval travel length considered in the interpretation procedure. Interval travel lengths for RRM, IM and DM are calculated to study its influence on the V_S determination as the waves travel through different interfaces.

Downhole test procedure

The downhole test is faster and more economical compared to the more detailed crosshole survey and provides better resolution than the surface wave methods. The standard procedure of the test follows ASTM (D7400-19 2019). The test utilizes an impact-based or vibration source to generate P- and S-waves on the surface (Kim et al. 2004a; Stokoe et al. 2008, 2017). A static load is placed on the source to ensure firm contact between the source and the ground. A vertical impact on a metal plate is used to generate P-waves, whereas a horizontally polarized excitation is used to generate horizontally polarized (SH) shear waves. In this study, the impact-based source included a horizontal wooden plank with steel end caps upon which a vertical static load is placed and a sledgehammer. Borehole geophone receivers BGK7 or BGK7 with directional control from Geotomographie GmBH were installed vertically with depth in the borehole and moved further after each record. Geode seismograph from Geometrics Inc. was used to record and digitize seismic waves. Waves were recorded at 0.125 ms sampling interval for a total record length of 1 s. Figure 1 shows the generation, travel path and particle motion of P- and S-waves in a typical downhole survey. As shown in Fig. 1, SH wave is captured best at the horizontal geophone oriented parallel to the particle motion or normal to the wave propagation direction, and P-wave is captured best by the vertical geophone (Roblee et al. 1994).

The arrival time of S-waves was determined using crossover method, which utilizes the polarity reversal characteristics of S-waves (Anbazhagan and Halder 2025; D7400-19 2019; Kim and Park 2002; Michaels 2001; Stokoe et al. 2008). Particle motion during the S-wave traverse follows the excitation polarity, and the direction of motion of particles reverses if the excitation direction is reversed. Thus, two oppositely polarized waveforms (generated using forward and reverse shots in Fig. 1) are used



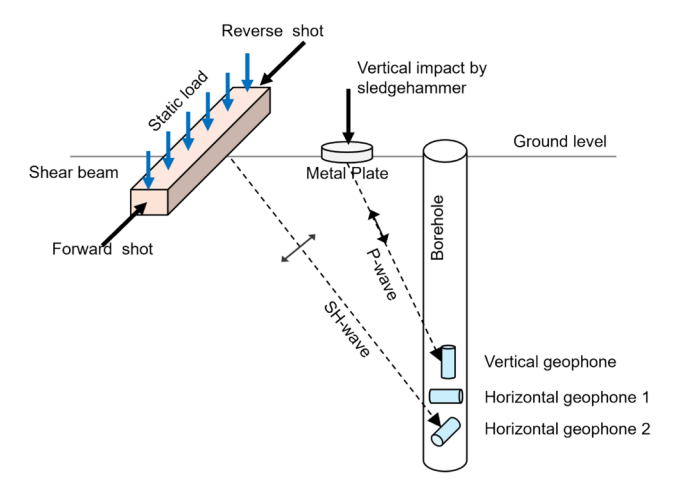


Fig. 1 Generation of P- and S-waves in seismic downhole test, wave paths marked in hatched lines and particle motion in solid lines with arrows

to determine S-wave arrival at a geophone stationed at a depth. Waveform polarity reversal is also accompanied by a reduction in frequency and an increase in amplitude (D7400-19 2019). Digital filters such as low-pass, high-pass and band-pass are often used to filter out the ambient vibrations, and mechanical and electrical interference is used from the signal. Typically, one of the horizontal geophones is oriented parallel to the direction of S-wave excitation for easy identification of S-wave arrival. In the absence of the direction of orientation of the geophone, principal component analysis is utilized to determine its orientation with respect to the source (Kim and Park 2002; Michaels 2001). Figure 2 shows a typical example

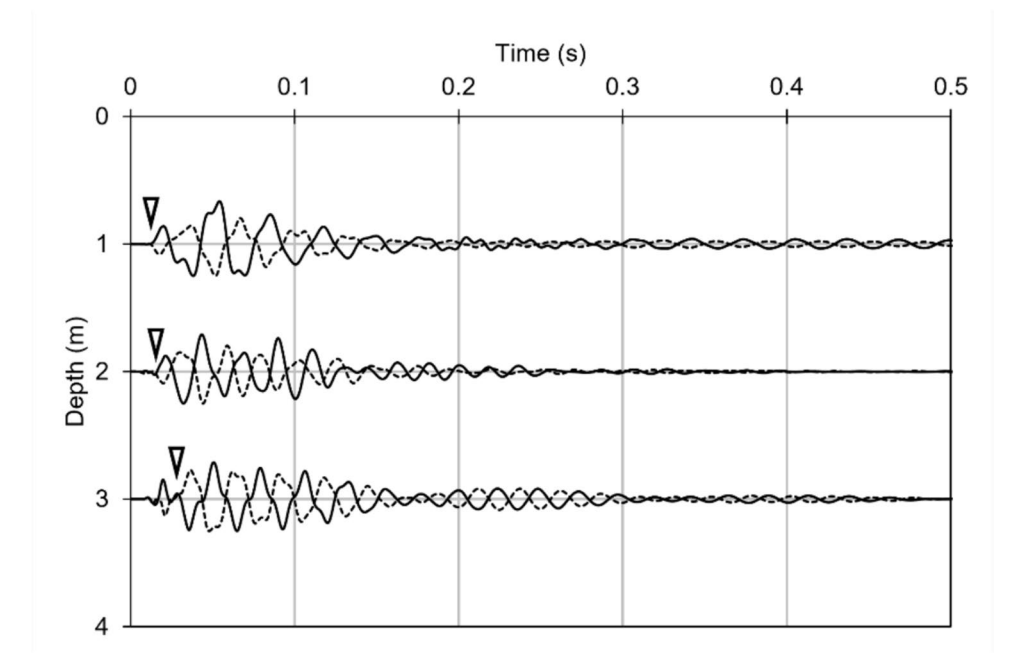
Fig. 2 Arrival times marked for typical S-wave signals in the downhole test using the crossover method. Forward and reverse waveforms are shown in solid and dashed lines, respectively of arrival time selection for SH-waves using forward and reverse excitation in the downhole survey.

Data reduction techniques for downhole tests

The downhole method interprets the velocity of body waves in the subsurface by measuring the arrival time of waves from the source to the receiver at different depths. After arrival times at all the depths are determined, a waterfall plot of depth versus arrival time is plotted and further used for velocity estimation. Common methods for interpretation are the direct method and interval method. Both methods do not consider refraction in the subsurface and assume a straight travel path from the source to the receiver. This assumption leads to quick determination of velocity profiles; however, it also causes misjudgment of velocity values at interfaces and anomalies, particularly in shallow depths (D7400-19 2019; Hallal and Cox 2019; Kim et al. 2004b). RRM is used to consider refractions at the layer interfaces, which gives a more realistic estimate of velocity (Bang et al. 2014; Boore and Thompson 2007; Kim et al. 2004b).

Direct method

The direct method is useful when the source-to-receiver distance is small, so the subsurface refraction can be neglected, and a straight raypath assumption stays valid (Bautista and Aguilar 2023b). First, the arrival time (t) is converted to the corrected arrival time (t_C) to project the travel path on the





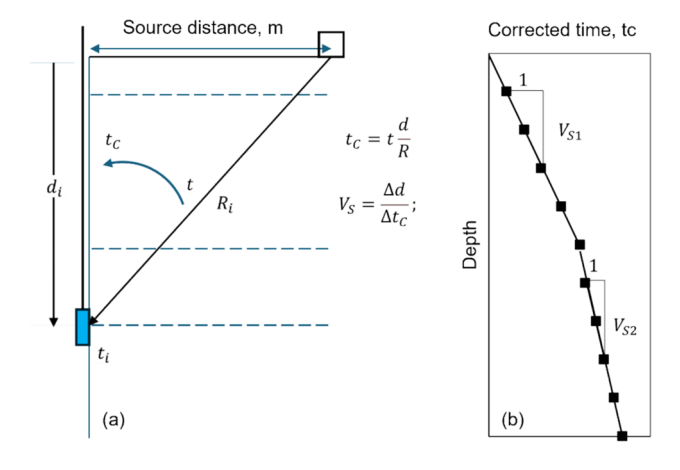


Fig. 3 Illustration of the direct method a Correction in arrival time \mathbf{b} V_S as slope of segments in corrected time-depth plot (after Kim et al. 2004a)

depth scale and thus remove the influence of refraction (Bang et al. 2014; Kim et al. 2004a; Stokoe et al. 2008) as shown in Fig. 3. The waterfall plot of corrected travel time versus depth is divided into several segments, and the slope of the linear plot between the two interfaces gives the V_S of the segment in between. This method results in an average V_S value for a subsurface layer between two interfaces. This can be helpful in the case of deeper deposits where a high-resolution profile is not desired and an average V_S profile will suffice (Kumar and Anbazhagan 2023; Stokoe et al. 2008). The workflow of the direct method is described in Eq. 1 and Fig. 3.

$$V_S = \frac{\Delta d}{\Delta t_C}; \quad t_C = t \frac{d}{R},\tag{1}$$

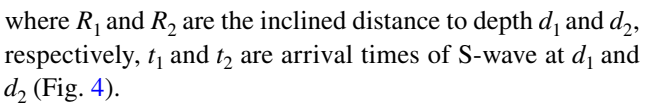
where Δd is the change in depth, and Δt_C is the change in the corrected arrival time.

The interfaces using the direct method can be selected manually from the borelog or from the plot by observing the linear trends between corrected arrival time and depth. A few algorithms have also been developed recently to automatically select interfaces to avoid ambiguity in interpretation (Bang et al. 2014; Boore and Thompson 2007).

Interval method

The interval method calculates $V_{\mathcal{S}}$ between the two depths by considering the differences in travel time and travel path length between them.

$$V_S = \frac{(R_2 - R_1)}{(t_2 - t_1)},\tag{2}$$



The interval method is useful when a high-resolution $V_{\rm S}$ profile is needed where velocity at each depth is known individually. However, this method does not work when the arrival time at any depth is less than the previous depth or the difference in arrival time between two successive depths is very small. In such cases, the velocity estimate turns out to be negative or unrealistically high (D7400-19 2019; Hallal and Cox 2019; Kim et al. 2004b). An example of such a case is discussed in this section. A 5-m deep model shown in Fig. 5a consists of an increasing V_S profile with change in V_S at every 1 m depth. The top 1 m of subsurface has V_S of 100 m/s with an increase of 50 m/s with each interface. The last layer between 4 and 5 m has V_S of 300 m/s. Seismic source is considered at a distance of 3 m from the borehole. The acquisition depth interval is taken as 1 m. When source is placed at sufficiently large distances, the change in V_S in shallow depths can lead to critical refraction at interface which can lead to head wave arriving at the receiver before the direct wave (Butler and Curro 1981; Daraei et al. 2024; Hallal and Cox 2019; Vergniault and Mari 2020). Figure 5b-d shows the arrival time of the head wave and direct

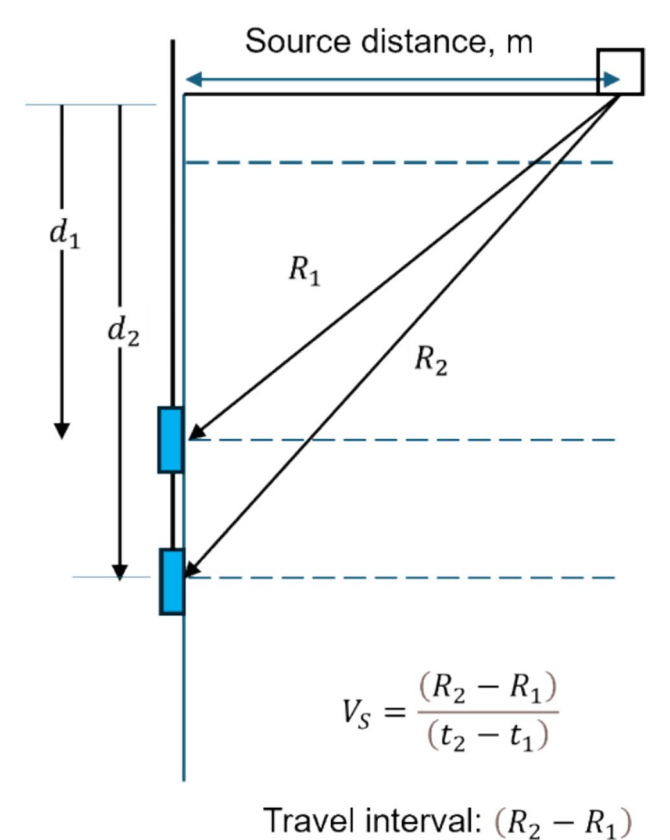
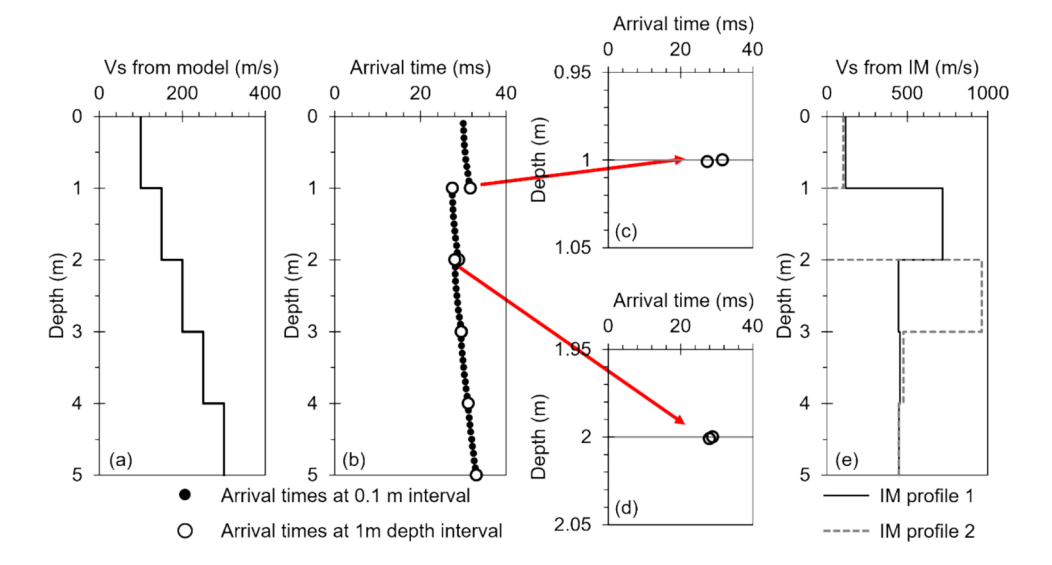


Fig. 4 Illustration of the interval method (D7400-19 2019; Hallal and

Cox 2019; Kim et al. 2004a)



Fig. 5 Illustration of ambiguity associated with interval method $\bf a$ model profile, $\bf b$ arrival time at different depths, along with arrival times obtained at 1 m depth interval, $\bf c$ two possible arrival times at 1 m depth due to change in V_S , $\bf d$ two possible arrival times at 2 m depth due to a change in V_S $\bf e$ two V_S profiles showing ambiguity in V_S profiles from IM due to high V_S before interface in one and negative V_S followed by high V_S in second profile



wave at 1 m and 2 m depth, which infer that head wave can mask the arrival of direct wave. Figure 5b also shows the arrival times at 0.1 m depth interval to highlight that arrival times show a sudden reduction at the interface and that can influence the interpretation using IM. In the case of direct wave measurement, the arrival time at 2 m can be seen as less than the arrival time at 1 m. Two V_S profiles, first determined using arrival time of critically refracted head waves (IM profile 1) and second (IM profile 2) from arrival time of direct waves are shown in Fig. 5e. IM profile 1 interprets high V_S (~700 m/s) above the interface, while IM profile 2 shows negative V_S at 2 m and V_S of ~1000 m/s at 3 m. Thus, IM can lead to misjudgment of stiffness and fluctuations in V_S profile around interfaces.

Any estimate of V_S needs the time of travel of the S-wave and the length of travel between the two depths. For this purpose, the interval method considers the difference in raypath lengths $(R_2 - R_1)$ and total travel times $(t_2 - t_1)$, which is not an accurate representation. Moreover, the influence of the shallower layers is not considered in the calculation of V_S of the following layers (Bang et al. 2014; Kim et al. 2004b).

Refracted raypath method

The refracted raypath method evaluates travel path and time for seismic wave in each layer before reaching the receiver by including subsurface refraction while estimating the V_S values for different layers (Bang et al. 2014; Bautista and Aguilar 2023b; Joh and Mok 1998; Kim et al. 2004b; Mok et al. 1989; Wang et al. 2021b). Snell's law is used to calculate the V_S values for the next layer after any interface. Another boundary condition with the distance of the source

to the receiver being kept constant is applied (Bang et al. 2014; Kim et al. 2004b; Mok et al. 1989). Then, the V_S of any layer is calculated with Eq. 3.

$$V_{Si} = \frac{L_{ii}}{t_{ii}} = \frac{L_{ii}}{t_i - \sum \frac{L_{ij}}{V_{Si}}},$$
(3)

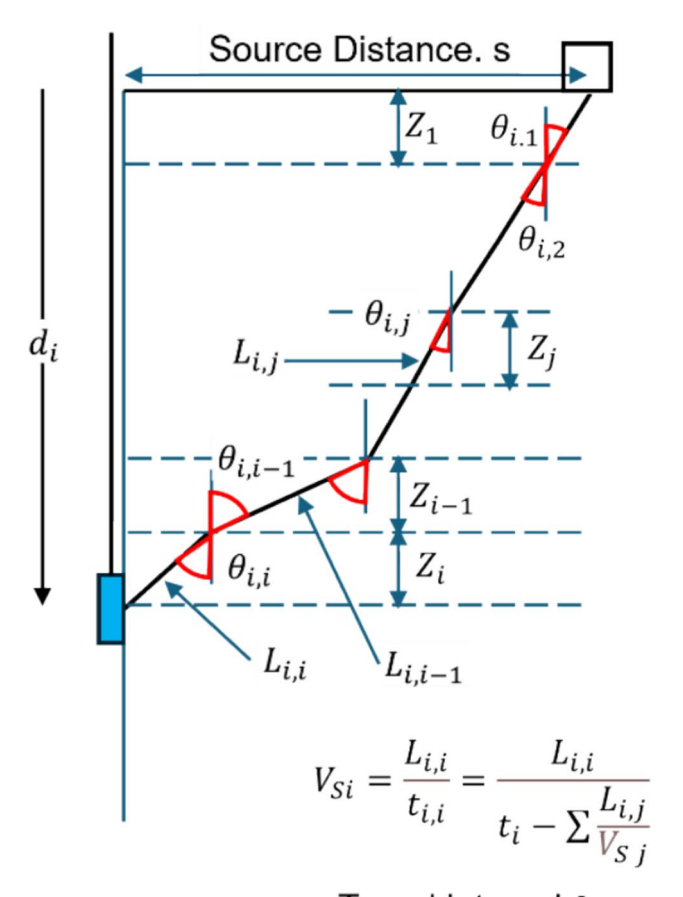
where $V_{Si} = V_S$ of the current layer, L_{ii} = raypath length in the *j*th layer during measurement at *i*th depth, $t_{i,j}$ = interval travel time in *j*th layer during measurement at *i*th depth.

As shown in Eq. 3 and Fig. 6, the estimation of V_S using RRM includes V_S of all the subsurface layers above the *i*th layer. The interval raypath length (L_{ij}) in each layer cannot be calculated directly using the direct travel path, rather its estimation will depend upon the V_S of the current layer as well as the previous layers as evident from Eq. 3.

Combined direct and interval method

As discussed above, conventional interpretation methods (DM and IM) have issues with overestimating or underestimating velocities. Further, RRM needs the estimate of V_S of upper layers to determine V_S of a particular layer, and the results are highly dependent on the initial input values (Wang et al. 2021b). This includes an iterative procedure to solve equations and boundary conditions, and any error encountered in one layer will also propagate to the deeper layers as well. Hence, here, an alternate method is proposed by combining direct and interval methods, which is called the combined direct and interval method (CDIM). As given in Eq. 1, the direct method estimates V_S as the slope of corrected travel time vs depth plot. Here, Δd and Δt_C are dependent upon the selection of interfaces. However, if





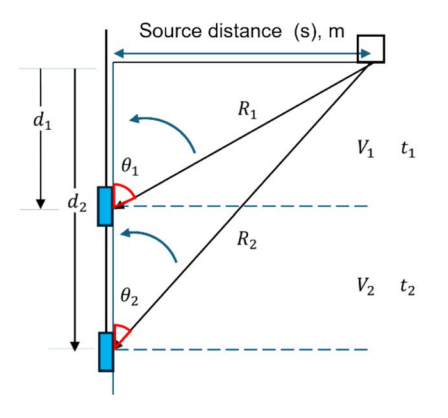
Travel interval: $L_{i,i}$

Fig. 6 Illustration of refracted raypath method (RRM) (based on Kim et al. 2004a)

we keep reducing these two parameters, the direct method will eventually converge to a form of interval method with $\Delta d \rightarrow \Delta d_i$.

$$V_{Si} = \lim_{\Delta d \to \Delta d_i} \frac{\Delta d}{\Delta t_c} = \frac{\Delta d_i}{\Delta t_{Ci}} = \frac{\left(d_i - d_{i-1}\right)}{\left(t_{ci} - t_{c(i-1)}\right)}.$$
 (4)

Fig. 7 Combining direct and interval methods for downhole interpretation



Corrected time (t_C) is estimated considering the vertical projection of the inclined travel path, which is the depth. Hence, Eq. 4 represents the interval method in the corrected time domain in the vertical direction. This alternate form does not require the calculation of V_S of any of the upper layers and can directly result in V_S of the *i*th layer (Fig. 7).

Figure 7 presents the derivation of the CDIM from the interval method discussed above. Same V_S can be obtained with and without considering the influence of V_S values of the previous layers. Equations A and B in Fig. 7 show both independence and dependence of V_S estimation upon the previous layers. To dive deeper into the efficacy of CDIM to determine V_S profiles, a simple subsurface model with two-layer subsurface is studied under varying magnitude and depth of V_S contrast. Further, field data from downhole surveys at five test locations are discussed.

Model study

Three subsurface models, each consisting of two layers are considered to study the effect of change in subsurface stiffness on V_S determination using IM and the proposed CDIM. The direct method (DM) is not considered here as two layers have constant V_S and DM would result in the same V_S as the model. The first layer has a V_S of 200 m/s (V_{S1}), whereas V_S of the second layer (V_{S2}) is varied from 100 to 600 m/s to determine the errors obtained in IM and CDIM in estimating V_S at interfaces. Snell's law is used to determine the arrival times for the three models at a testing depth interval of 1 m, with a source distance of 2 m.

The first model contains two layers of a total depth of 5m with an interface at 3 m depth (Fig. 8). The arrival times for S-waves are plotted in Fig. 8a. The V_S profiles from IM and CDIM are compared against the model for relative error at the depths below the interface (4 m and 5 m). Critical refraction at the interface for $V_{S2} \ge 400$ m/s was observed; hence for these V_{S2} values, errors above interface at 3 m depth is also evaluated. The V_S profiles from IM and CDIM are shown in Fig. 8b and c. As evident from Fig. 8b, the first

From interval method:

$$V_2 = \frac{R_2 - R_1}{t_{2,} - t_1}$$

Proceeding as direct method:

$$V_2 = \frac{\Delta d}{\Delta t_c} = \frac{d_2 - d_1}{t_{c2} - t_{c1}} = \frac{d_{2,2}}{t_{c2,2}} \tag{A}$$

$$= \frac{R_{2,2}\cos\theta_2}{t_{2,2}\cos\theta_2} = \frac{R_{2,2}}{t_{2,2}} = \frac{R_{2,2}}{t_2 - \frac{R_{2,1}}{V_{\text{C},1}}}$$
(B)



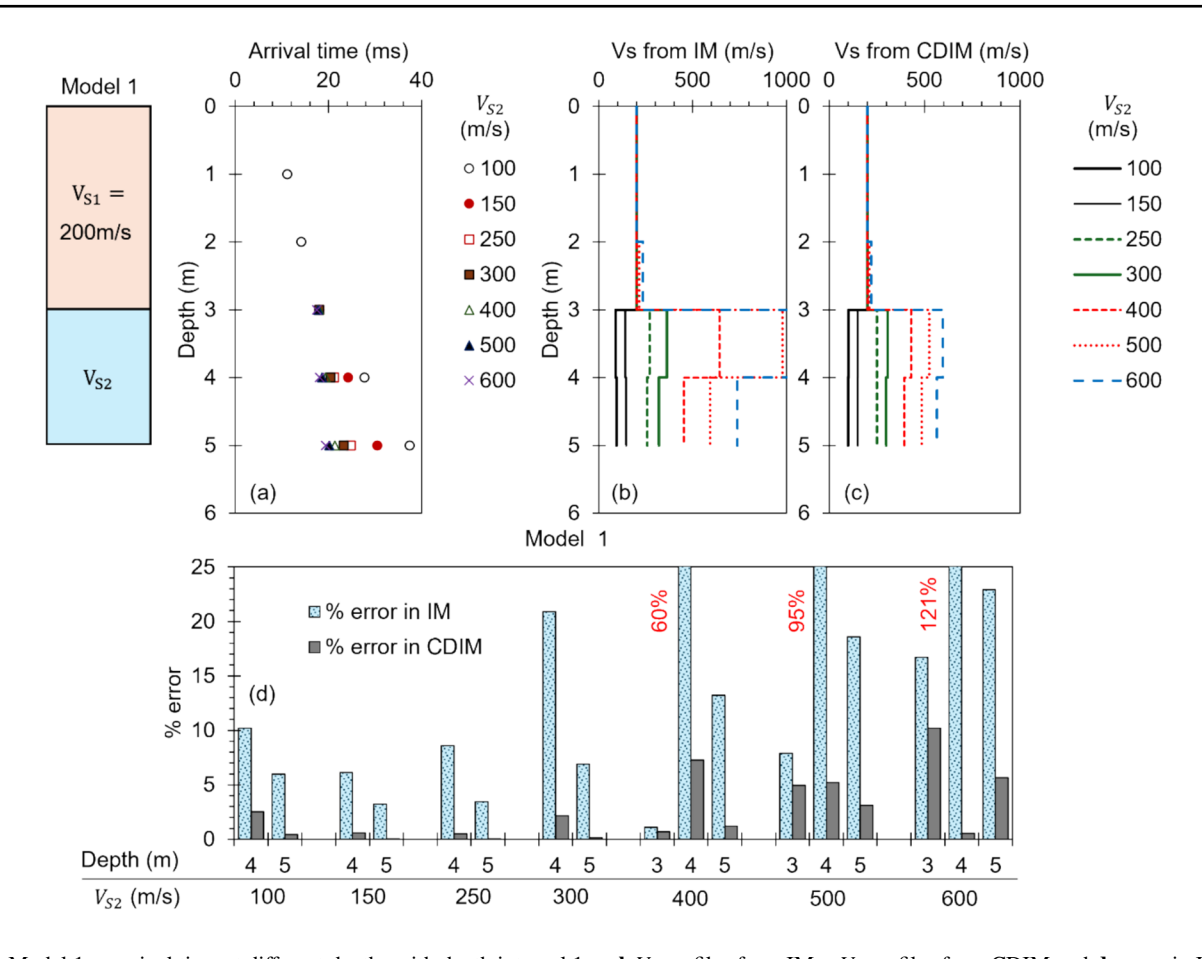


Fig. 8 Model 1, $\bf a$ arrival time at different depths with depth interval 1 m, $\bf b$ V_S profiles from IM, $\bf c$ V_S profiles from CDIM and $\bf d$ errors in IM and CDIM profiles relative to RRM

record below the interface is highly prone to misinterpretation, with an estimate of V_{S2} reaching 1300 m/s for model V_{S2} 600 m/s. IM shows a high error of over 20% when V_{S2} is 300 m/s, and the error increases to 60% for $V_{S2} = 400$ m/s, 95% for $V_{S2} = 500$ m/s and 120% for $V_{S2} = 600$ m/s. When $V_{\rm S2} < V_{\rm S1}$, the error at 4 m depth from IM profile is between 5 to 10% and V_{S2} is underestimated. The second acquisition depth below the interface shows smaller errors when V_{s2} exceeds V_{S1} , however for higher V_S contrasts the error at 5m reaches 22%. For $V_{S2} = 600$ m/s, error above interface is about 16%. CDIM shows negligible error at 4m depth for $V_{S2} < V_{S1}$ conditions; the error is well within 20% up to $V_{S2} = 500$ m/s, and increases to 37% for $V_{S2} = 600$ m/s. The maximum error above the interface is observed to be 10% at $V_{s2} = 600$ m/s. Thus, the error in the CDIM is confined just below the interface for high V_{S2} contrast, while the error in IM can be observed above the interface as well and also propagates to the second depth of acquisition below the interface. The comparison of errors from IM and CDIM is summarized in Fig. 8d.

The second model consists of two layers of a total depth of 10 m with an interface at 8 m depth (Fig. 9). Figure 9a

shows arrival time for S-wave for the model for different V_{S2} values. V_S profiles from Fig. 9b and c show that errors have significantly reduced compared to model 1 even for higher V_{S2} values as the interface depth has increased. At 9 m, the errors from IM reach 22% for V_{S2} =600 m/s, while from CDIM it barely exceeds 8%. Errors observed in the estimation of V_{S2} from IM and CDIM are summarized in Fig. 9d.

The third model consists of a two-layer system with a total depth of 15 m and an interface at 13 m depth (Fig. 10). Arrival time for S-waves at different depths, V_S profile from IM and V_S profile from CDIM are shown in Fig. 10a–c, respectively. Figure 10d shows the improvement obtained over IM using CDIM in model 3. It is clear that with the increase in depth of the interfaces, the errors in both IM and CDIM have reduced and fallen within the 10% margin. CDIM shows much lower errors with most of them confined less than 2%, while IM still shows up to 8% deviation from the model. For lower V_{S2} values, both IM and CDIM result into similar V_S profiles.

This model study results in two observations. First, the influence of interfaces reduces with depth, and second, the CDIM estimates V_S with significantly less error when



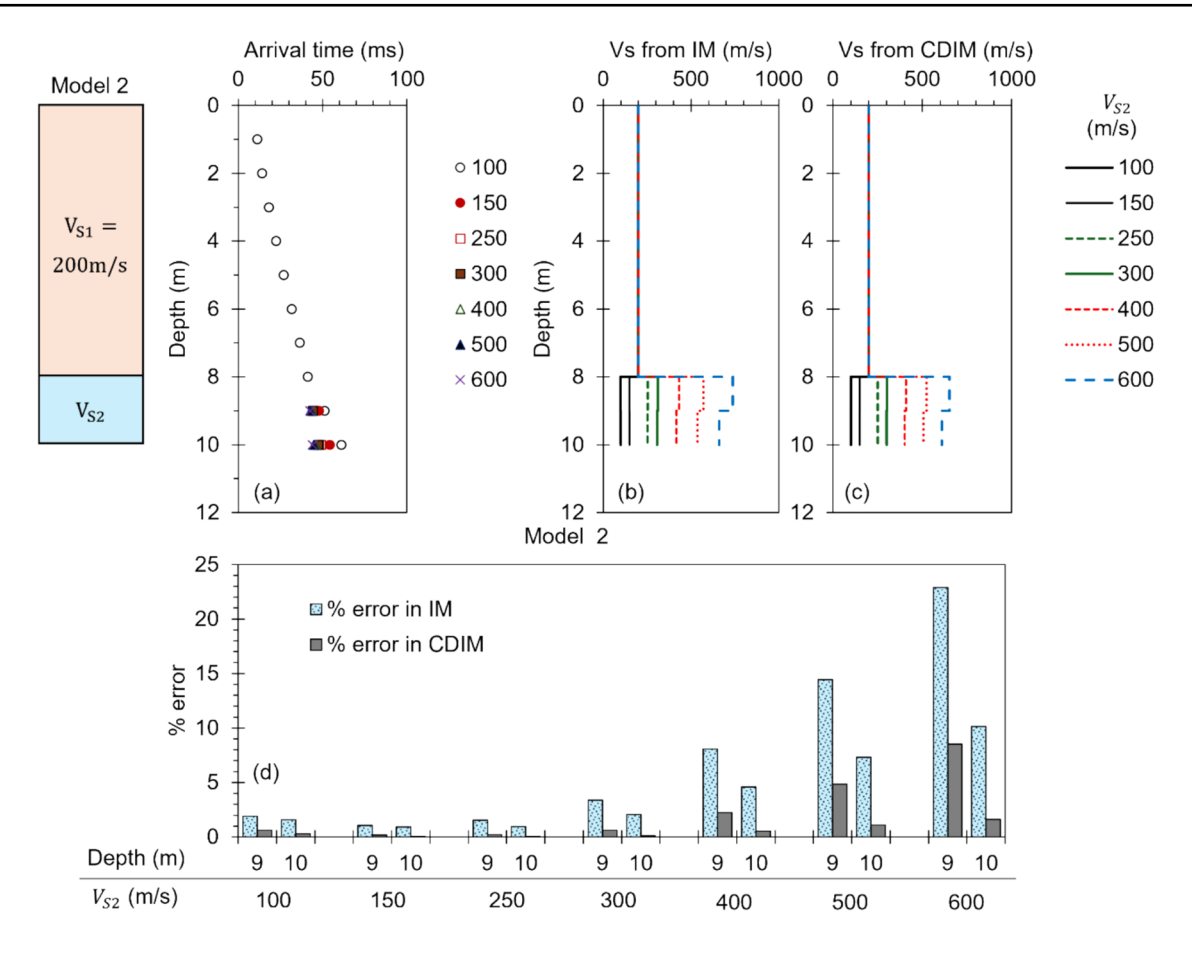


Fig. 9 Model 2, $\bf a$ arrival time at different depths with depth interval 1 m, $\bf b$ V_S profiles from IM, $\bf c$ V_S profiles from CDIM and $\bf d$ errors in IM and CDIM profiles relative to RRM

compared to IM. One instance of high error from CDIM is noted when V_{S2} increases to three times V_{S1} in shallow depth. The following section discusses the application of CDIM using field data acquired from downhole tests.

Field testing and application of CDIM

After the model discussed above established the efficacy of CDIM, field test data were analyzed to observe its performance against IM in various subsurface conditions. Since CDIM is proposed as a simplified procedure, for analysis purposes V_S profile from RRM is considered as a reference profile as RRM involves V_S estimation using refracted raypaths and application of Snell's law. The errors in CDIM and IM are compared against the change in V_S at interfaces, as discussed in the previous section as well. Figure 11 shows the subsurface lithology determined at the downhole test locations.

Test site C9 is a coastal alluvial deposit with silty sand and clayey subsurface deposits underlain by a shale rock stratum. Test site BBSR5 consists of cemented lateritic formations. Test site CTR1 lies in the residual deposit region with predominantly silty strata over gneiss and charnockite layers. Test site TCN is in a coastal alluvial deposit close to the seashore with silty sand underlain by weathered sandstone and limestone strata. Test site B4 lies in a residual soil region with silty sand as predominant sediment with gneiss and granitic bedrocks. The source distance at the test locations varied between 2 to 3 m, based on the space availability near the boreholes. A wooden beam of length 2 m, capped at the end with steel plates, was used as the source. A sledgehammer was used for impact at the ends of the beam. A surcharge weight was used to keep the beam in position to ensure contact between the beam and the ground.

Discussion on field experiments

Error in V_s estimation by DM, IM and CDIM

For the estimation of V_S profiles, the arrival times of S-wave at different depths were determined from the crossover method as discussed previously. The arrival



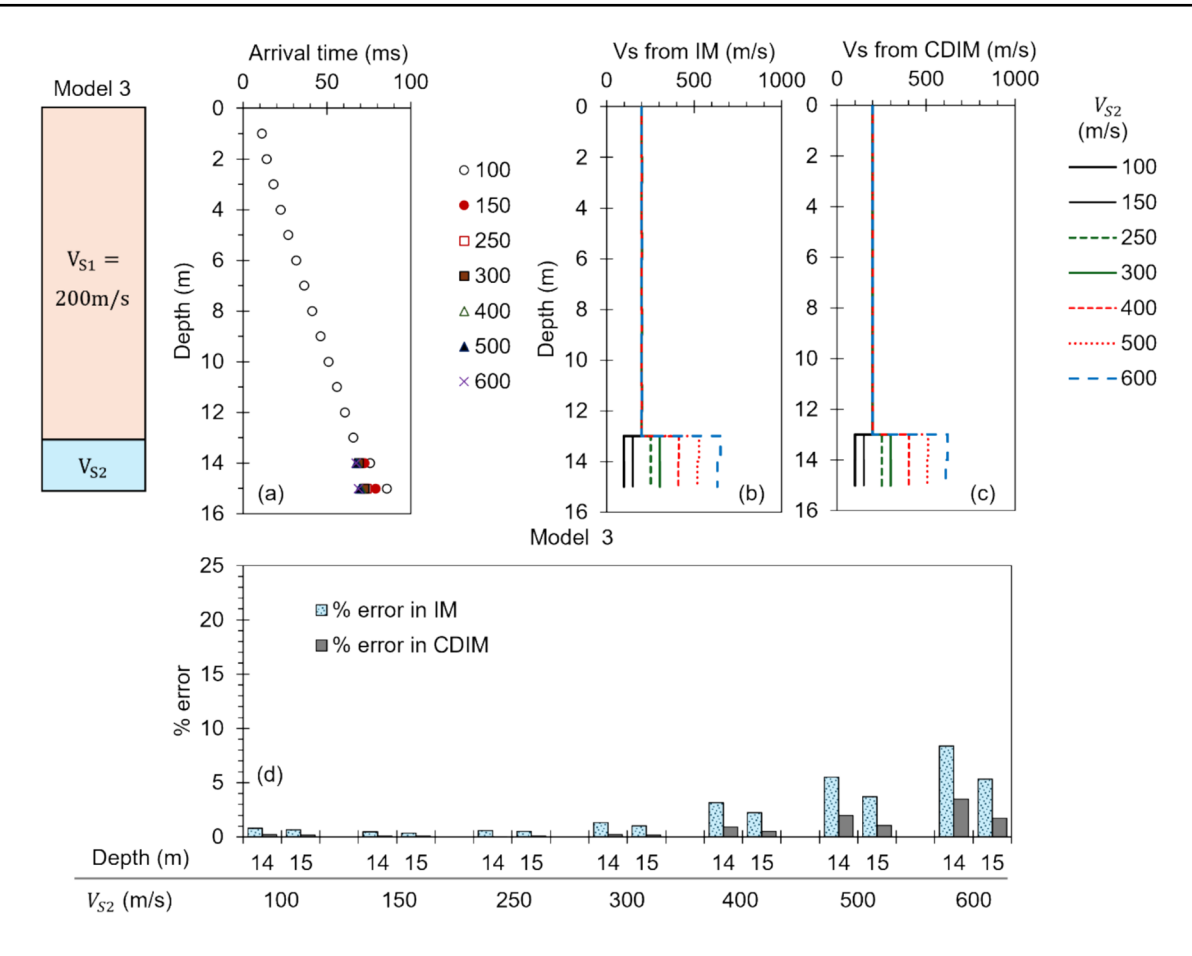


Fig. 10 Model 3, a arrival time at different depths with depth interval 1 m, b V_S profiles from IM, c V_S profiles from CDIM and d errors in IM and CDIM profiles relative to RRM

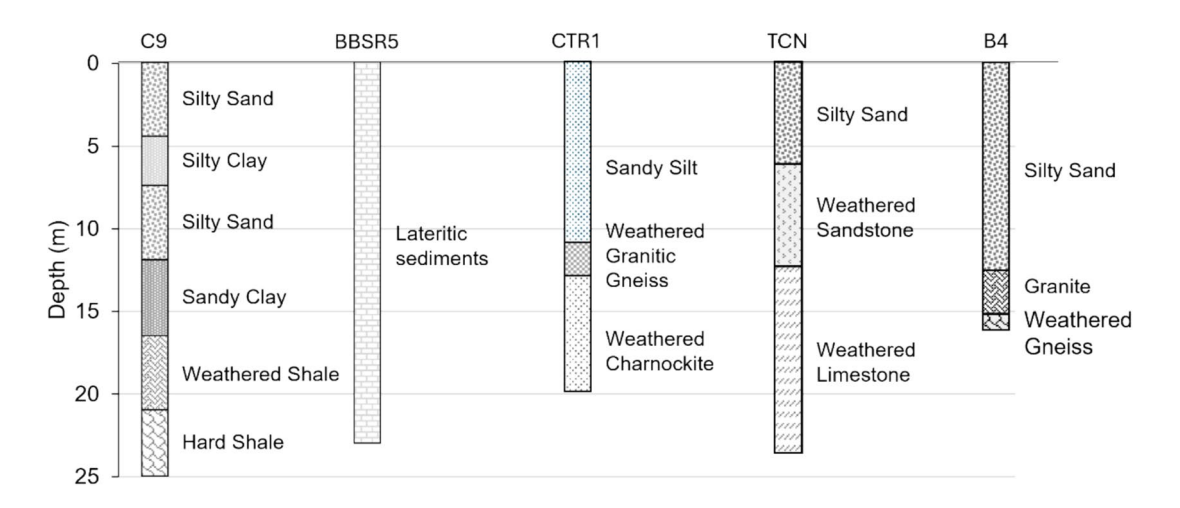


Fig. 11 Borelogs at five test locations

times were then corrected for the vertical direction and further V_S was estimated using the DM, IM and CDIM. For V_S estimation from DM, a threshold of 0.99 for R^2 was considered in corrected time-depth plot for interface

selection. V_S from the RRM was also calculated to consider the accurate travel paths in the subsurface and obtain the deviation of both IM and CDIM from RRM.



At test location C9, there are layers of sandy soil up to 13 m, followed by weathered charnockite rocks. The source distance was kept at 2.3 m. The arrival time versus depth plot shows the presence of a low V_S layer in the top 5m, below which the V_s increases (Fig. 12a). In shallow depths, the V_S plots from IM and CDIM show minor differences (Fig. 12c); however, at deeper depths beyond 10m, both are almost equal. DM results into an average profile which does not capture the sudden changes in V_S with depth (Fig. 12b). When comparing V_S from RRM with V_S from CDIM, V_S profiles from both methods result in almost similar values. The depths where the interval method resulted in much higher values, CDIM is giving closer values to RRM (Fig. 12d). The interval method is unable to fully resolve V_{S} at the depths with a high V_S contrast. As the depth increases, V_S profiles from the three methods result in similar V_S profiles. Figure 12e shows the errors observed in V_S profiles from CDIM, DM and IM when compared to RRM. As evident from V_S profiles as well, errors from IM in shallow depths are high ranging up to 30%. Similarly with DM, the errors are over 20% within 10m and below 20 m where fluctuations in V_s profiles are observed.

At test location BBSR5, the subsurface is cemented laterite which has zero rock quality designation (RQD)(Deere and Deere 1988) throughout depth. The source distance at this site was 2.8 m from the borehole. Figure 13a shows the arrival time graph, with low time intervals at 2 m, 4 m and 14 m. As shown in Fig. 13b–d, IM shows three spikes in V_S values, out of which only one is observed in RRM and CDIM. DM shows average V_S for the depths between the interfaces, which are off from RRM profile by over 10% in most depths (Fig. 13e). At 14m depth, such high V_S value is probably a result of the local presence of weathered rocks

or gravel mix, resulting in the low difference in arrival time from the previous layer. Throughout the depth, RRM and CDIM result in similar V_S profiles, whereas the Interval method has high deviations from RRM in shallow depth and at the noted high impedance contrast. Error in the estimation of V_S from IM exceeds 100% at 2 m depth and is close to 50% at 4 m depth. As discussed previously, the errors from DM go as high as 30–40% at some depths.

At the test location CTR1, the subsurface consists of sandy silt soil layers followed by weathered gneiss and charnockite deposits. A source distance of 3 m from the receiver borehole was adopted. The arrival time for the first three recording depths shows a decreasing trend and then starts increasing (Fig. 14a). Thus, in shallow near-surface profiles, IM results in negative V_S values, whereas CDIM profiles compare well with the RRM profile (Fig. 14b, d). V_S from DM mostly stays within 10% error (Fig. 14c). Figure 14e shows the errors observed in V_S profiles from CDIM, DM and IM when compared to RRM. The negative V_S values at 2 m and 3 m depth lead to high errors in IM, whereas V_S from CDIM stays within 10% of RRM.

At the test location TCN, the borelog shows the presence of a silty sand alluvium layer followed by layers of sedimentary rocks, like sandstone and limestone, present in a weathered state. The source was placed at 3 m distance from the borehole. At 2 m depth, the arrival time is less than the arrival time at 1 m, hence IM results in negative V_S (Fig. 15a, b), which further leads to negative V_S at 3 m (Fig. 15b). Further, at all the depths, IM overestimates V_S , most notably at 4 m and 6–10 m. Between 5 and 15 m depths, DM compares well with RRM due to a uniform V_S value (Fig. 15c) but misses the increase in V_S toward the end of the profile. Compared to RRM, CDIM results in similar V_S except a minor

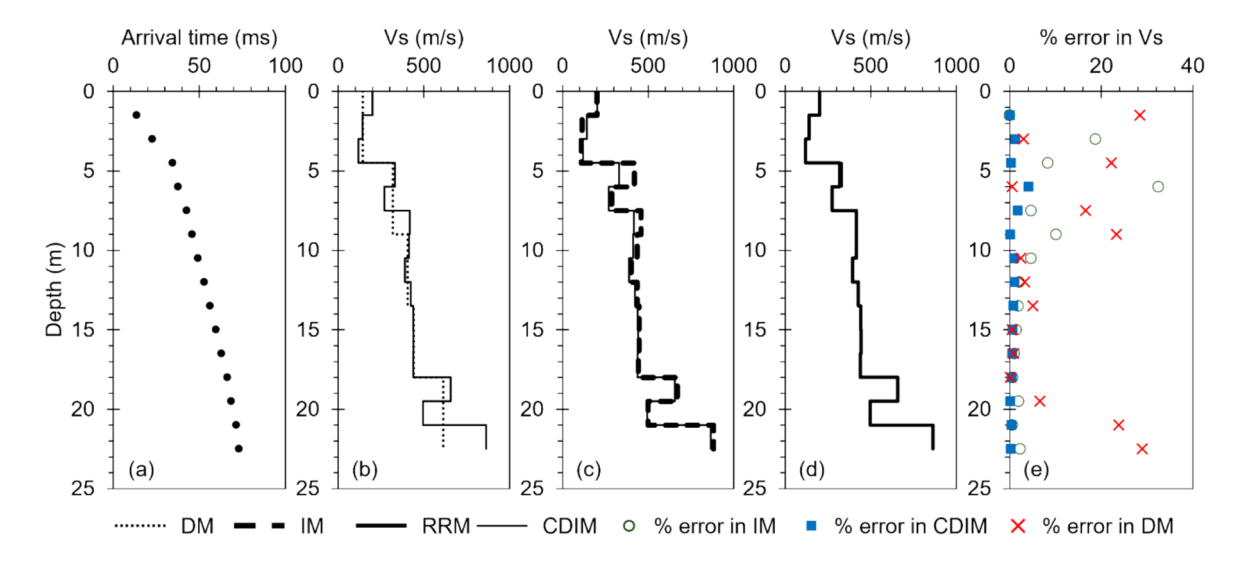


Fig. 12 a Arrival time of S-waves at different depths at C9; CDIM profile compared against, b DM, c IM and d RRM and e % error observed in DM, IM and CDIM when compared to RRM



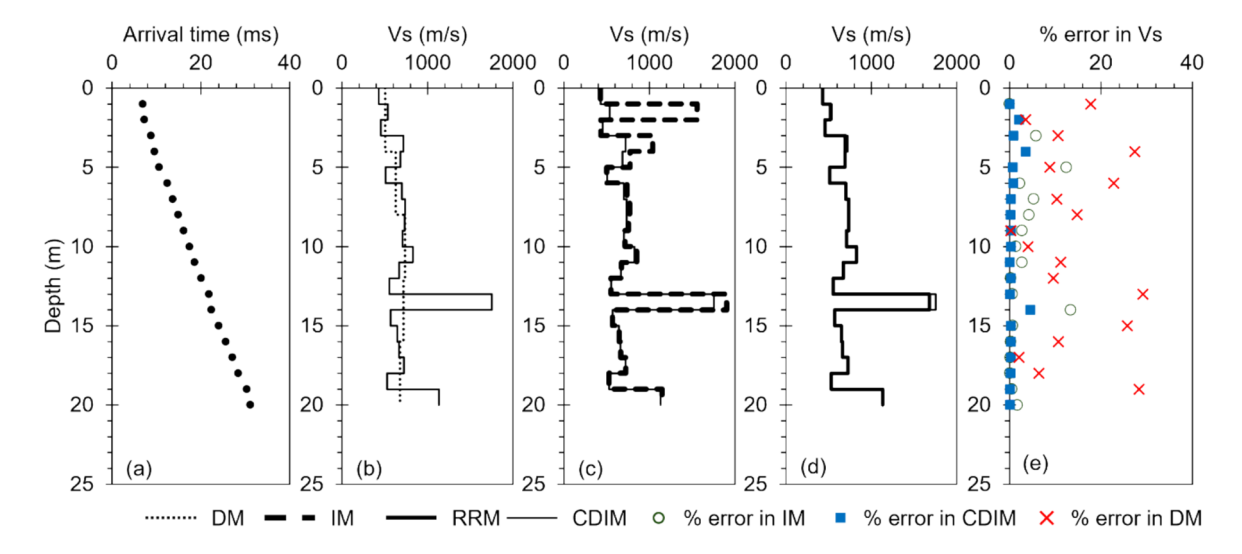


Fig. 13 a Arrival time of S-waves at different depths at BBSR5; CDIM profile compared against b DM, c IM and d RRM and e % error observed in DM, IM and CDIM when compared to RRM

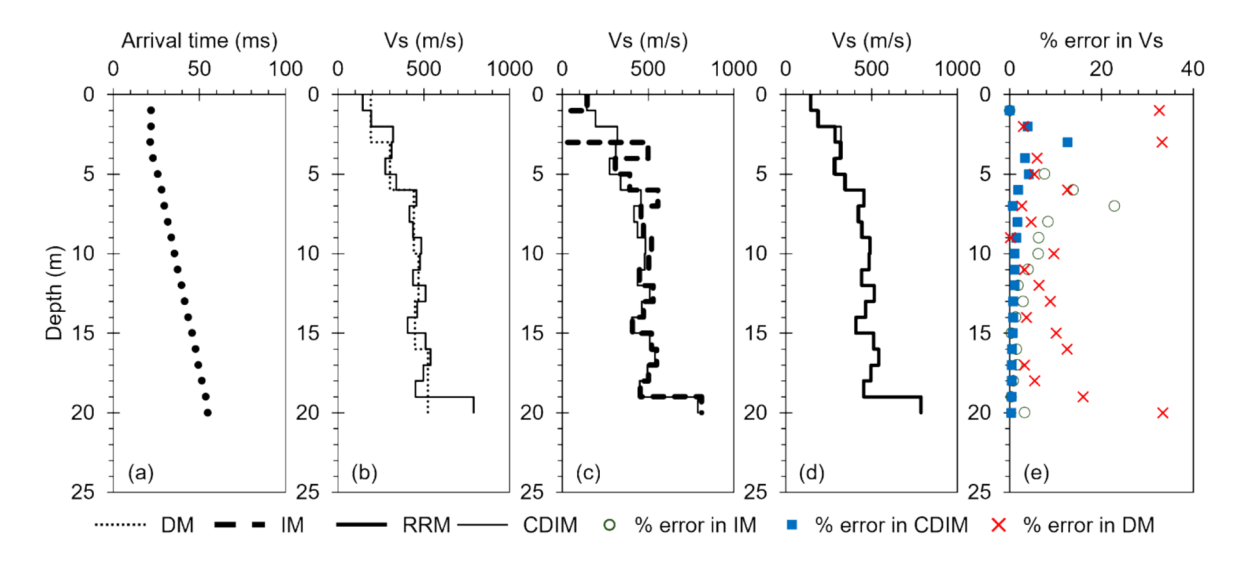


Fig. 14 a Arrival time of S-waves at different depths at CTR1; CDIM profile compared against b DM, c IM and d RRM e % error observed in DM, IM and CDIM when compared to RRM

deviation at 2 m depth where the arrival time reduction is noted (Fig. 15d). Figure 15e shows the errors observed in V_S profiles from CDIM, DM and IM when compared to RRM. At 2 m depth, due to negative V_S from IM the associated error is as high as 300%. Subsequent depths show smaller errors but still between 10 and 30%. DM also shows errors over 20% in shallow depths and below 15 m.

The test site at B4 consists of silty sand followed by weathered gneiss rock formations. The source was placed at 3.45 m from the borehole. Because of the very low time interval in arrival time from 1 to 3 m, IM results in very high V_S values from 1 to 3 m (Fig. 16a, c). Below 5 m depth, V_S values from IM are higher compared to CDIM or RRM. The

continuous increase and decrease in V_S profile is captured by RRM and CDIM as well but IM shows higher V_S values (Fig. 16b–d). DM shows more intermediate V_S values which are average between two interfaces (Fig. 16b). Figure 16e shows the errors observed in V_S profiles from CDIM, DM and IM when compared to RRM. Due to high V_S estimated at 2 m and 3 m depth, the associated errors exceed 100% in IM. Similarly, DM cannot capture the fluctuating V_S profile, and shows 10–30% error in estimation.

From these five field studies, it can be observed that the interval method is very sensitive to the difference between the arrival time at two subsequent depths and leads to very high and often negative V_S values at high V_S contrasts and



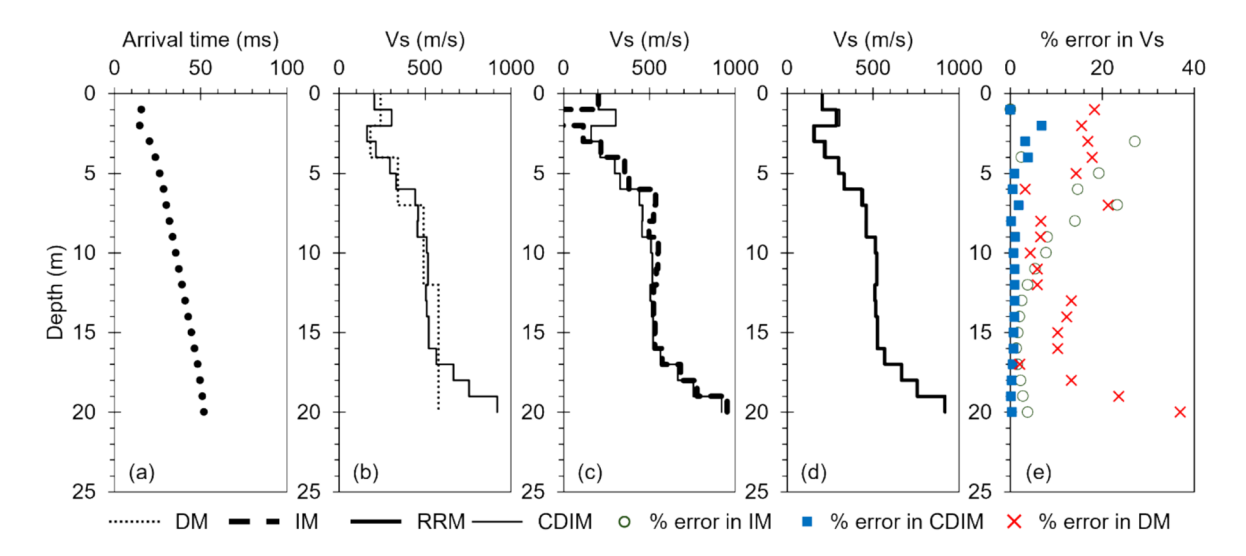


Fig. 15 a Arrival time of S-waves at different depths at TCN; CDIM profile compared against b DM, c IM and d RRM and e % error observed in DM, IM and CDIM when compared to RRM

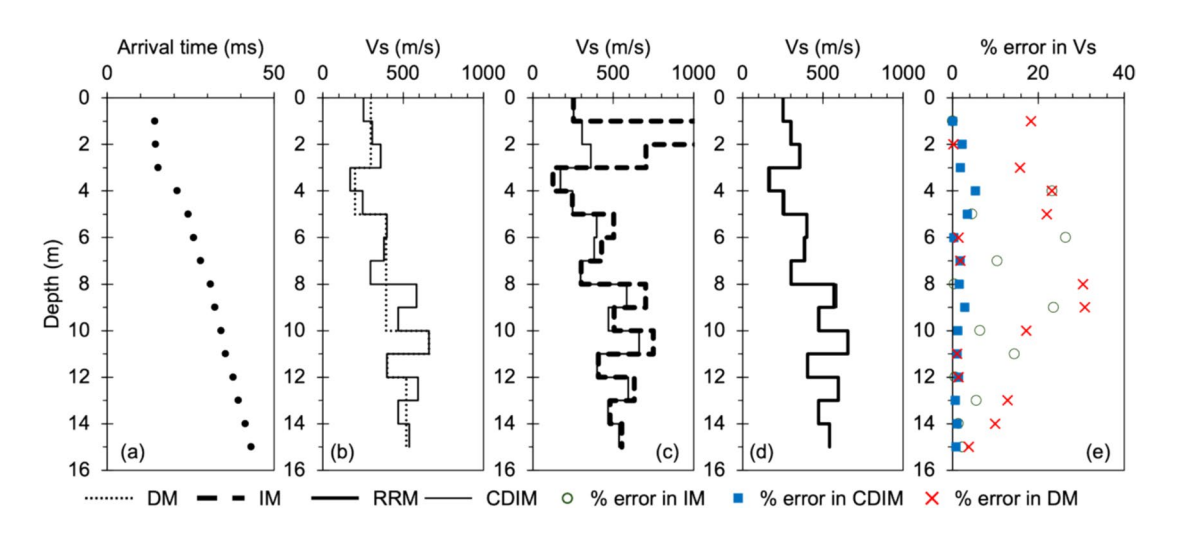


Fig. 16 a Arrival time of S-waves at different depths at B4; CDIM profile compared against b DM, c IM and d RRM and e % error observed in DM, IM and CDIM when compared to RRM

thin layered high V_S anomalies. However, this observation is mostly confined to the shallow depths. When comparing both IM and CDIM profiles with DM, CDIM results are closer to DM as CDIM is derived from DM by converging the thickness of a soil segment to the depth interval. Another important finding is the convergence of both IM and CDIM profiles with RRM profile within a 10% error margin (mostly within 5%) as the depth increases.

In these field investigation, RRM profiles are used as reference, since RRM considers refraction and influence of all the subsurface layers above to estimate V_S . In all these field studies, CDIM compares well with RRM, which ascertains the reliability of CDIM and CDIM is computationally much less extensive than RRM. Test results at C9, TCN and B4

are also compared with available crosshole data in Fig. 17. At C9 (Fig. 17a), crosshole shows lower V_S than the DH profiles in 5m to 15m depth range, which consists of fine-rich alluvial deposits. The difference in V_S is quite high and is also discussed in Kumar and Anbazhagan (2025). V_S profiles from DH and crosshole agree well at TCN (Fig. 17b) and B4 (Fig. 17c).

Interval travel lengths for RRM, IM and CDIM

The interval travel length considered between the two depths directly affects the further estimation of V_S . With the increase in depth, the raypath becomes nearly vertical, and



Fig. 17 Comparison of all DH profiles against crosshole data at a C9, b TCN and c B4

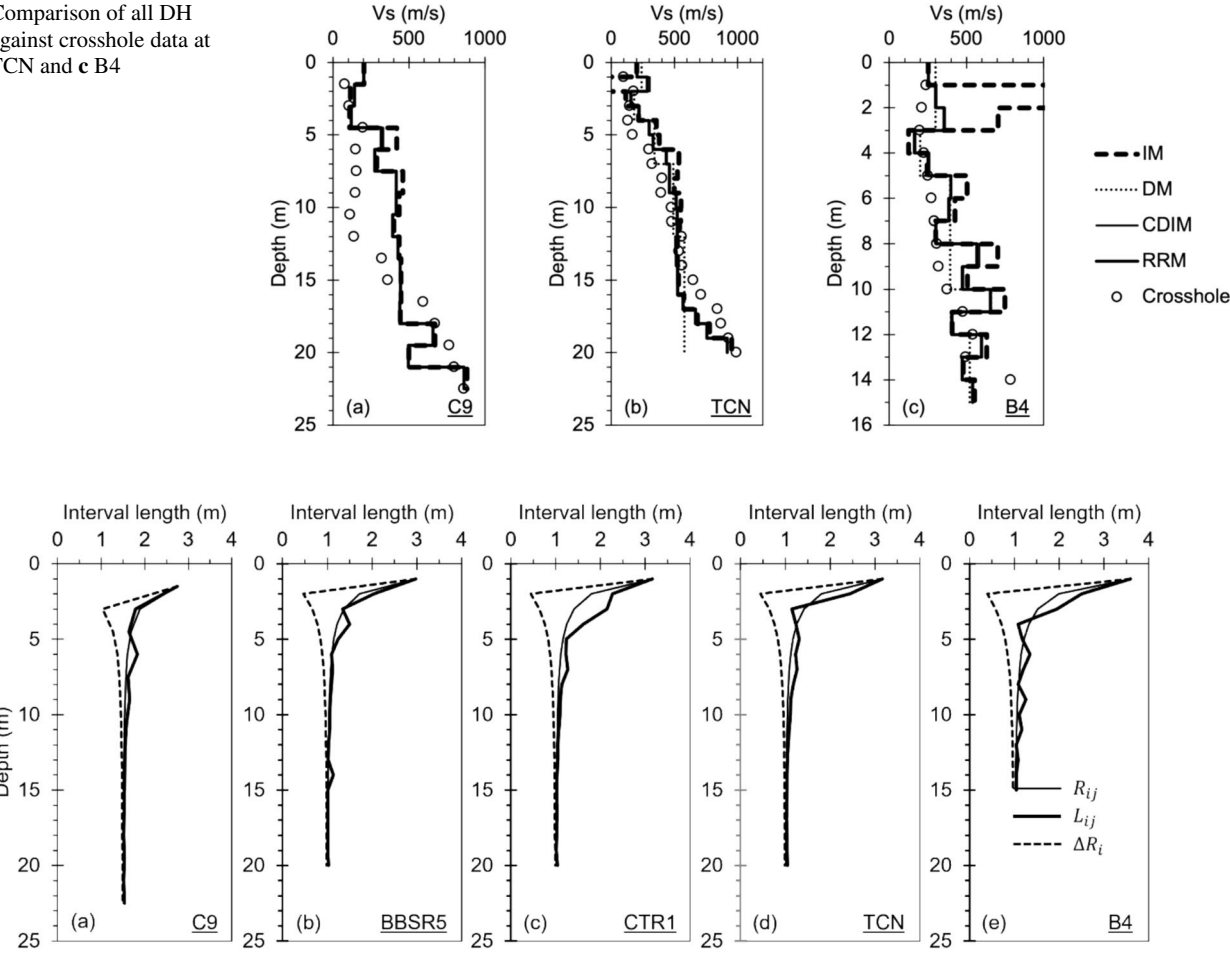


Fig. 18 Interval travel lengths at different depths obtained from considering different travel paths: inclined (R_{ii}) , refracted (L_{ii}) and inclined difference (ΔR_i) at test locations

the interval travel length between the two depths becomes equal to the depth interval. Figure 18 shows the different interval travel lengths and their variation with depth at the five test locations. The interval lengths shown are the lengths of inclined raypath in the *i*th layer (R_{ij}) , the length of refracted raypath in the *i*th layer $(L_{i,i})$ and the difference in inclined raypath lengths (R_i, R_{i-1}) between ith and (i-1)th depth (ΔR_i). The interval lengths converge to the depth interval beyond 10 m in all the field locations, except B4 where it occurs after 12 m. The maximum difference in the interval length is observed at the second depth of acquisition, where IM is applied for the first time. Interval travel length for CDIM will be Δd which is constant for all the depths. The interval lengths from the three estimates are the same for the first depth as the direct raypath length from the source to the first depth of acquisition.

The interval path length changes at higher depths if a thin layer of high impedance contrast is observed, as in BBSR5 at 14-15 depth and at several depths at B4. Otherwise, the interval travel length remains close to the interval depth.

As discussed earlier as well, the interval travel lengths are affected more by refraction in the shallow depths and much less in the deeper depths. This observation also reinforces the finding that shallow depth is more susceptible to changes in $V_{\rm S}$ profiles with the change in interpretation method. With an increase in depth, the V_S profiles become less susceptible to such changes. Thus, V_S profiles from different interpretation methods will eventually converge at higher depths.

Conclusions

This study discusses the application of the interval method and direct method for interpreting downhole data. The direct method was modified to obtain a form of interval method for better interpretation of downhole tests for V_{ς} profiles. In shallow depths, the interval method showed errors in V_S estimation which was improved by considering the combination of direct and interval method, i.e., CDIM. More detailed refracted raypath method (RRM) involves the



calculation of raypath length and time of travel in each layer above the concerned layer, which is not needed for CDIM and the V_S can be estimated directly by correcting the arrival time for depth in the vertical direction. Thus, V_S profiles can be determined with much ease and sufficient accuracy. The efficacy of CDIM was validated by three model studies and five field downhole studies. When compared with RRM, CDIM resulted in fairly accurate V_s profiles within 10% error margin (which in most cases is less than 5%) and is observed to be a simplified reduction procedure with much less time complexity. In the presence of high impedance contrasts and V_S anomalies in the shallow depths, CDIM results in small deviations from RRM. With increasing depth, V_S profile from CDIM is affected only due to high impedance contrast, which is also reflected in the interval travel lengths measured. As the depth increases, IM, RRM and CDIM lead to almost equal interval travel lengths as the raypaths become vertical, and interval travel lengths converge to depth interval. Another observation in the case of IM was that the interval travel length is least for the second depth of acquisition, and then it increases and approaches the value of depth interval, whereas for RRM, it shows a decreasing trend from the maximum at the first depth to the depth interval magnitude after a certain depth. This finding supports the observation of similar V_S values at greater depths.

Acknowledgements This work was supported by the Dam Safety (Rehabilitation) Directorate, Central Water Commission, Govt. of India for the project entitled "Capacity Buildings in Dam Safety" under Dam Rehabilitation and Improvement Project"; SERB, DST, Govt. of India for the project "Development of correction factors for standard penetration test N values in India through energy measurement and field experiments—Step toward a reliable Liquefaction Potential Assessment" under Grant SERB/F/198/2017-18 dated 11/05/2017; and M/s Secon Pvt. Ltd. for the project "Effect of shear wave velocity calibration on Amplification of shallow and deep soil sites" under grant SECON/IISc/MoES/WO/07-18/0079. The authors gratefully acknowledge the contributions of Kamalhassan, Ravinesh Kumar, Siriwanth Kumar and Divyasree for their invaluable assistance in field testing and data processing.

Declarations

Competing interests The authors declare that they have no known competing financial interests or personal relationships that could have appeared to influence the work reported in this paper. Financial and travel supports received for this study are mentioned in the Acknowledgements section.

References

- Anbazhagan P (2018) Subsurface investigation—integrated and modern approach, pp 245–257
- Anbazhagan P, Halder S (2025) A novel algorithm for identifying arrival times of P and S waves in seismic borehole surveys. Comput Geosci 194:105746

- Anbazhagan P, Kumar A, Yadhunandan ME, Siriwanth K, Suryanarayana K, Sahodar G (2022) Effective use of SPT: hammer energy measurement and integrated subsurface investigation. Indian Geotech J 52(5):1079–1096
- Anomohanran O (2013) Downhole seismic refraction survey of weathered layer characteristics in Escravos, Nigeria. Am J Appl Sci 11(3):371–380
- Bajaj K, Anbazhagan P (2021) Identification of shear modulus reduction and damping curve for deep and shallow sites: kik-net data. J Earthq Eng 25(13):2668–2696
- Bajaj K, Anbazhagan P (2023) Effective input velocity and depth for deep and shallow sites for site response analysis. Geomech Geoeng 18(3):193–207
- Bang ES, Cho SJ, Kim DS (2014) Mean refracted ray path method for reliable downhole seismic data interpretations. Soil Dyn Earthq Eng 65:214–223
- Bautista P, Aguilar Z (2023a) Interpretation methods for seismic downhole test in inclined boreholes. Civ Eng J 9(10):2592–2611
- Bautista P, Aguilar Z (2023b) Interpretation methods for seismic downhole test in inclined boreholes. Civil Eng J 9(10):2592–2611
- Boore DM (2016) Determining generic velocity and density models for crustal amplification calculations, with an update of the Boore and Joyner (1997) generic site amplification for Vs(Z) = m/s. Bull Seismol Soc Am 106(1):316–320
- Boore DM, Asten MW (2008) Comparisons of shear-wave slowness in the Santa Clara Valley, California using blind interpretations of data from invasive and noninvasive methods. Bull Seismol Soc Am 98(4):1983–2003
- Boore DM, Gibbs JF, Joyner WB (2021) Damping values derived from surface-source, downhole-receiver measurements at 22 sites in the san francisco bay area of central california and the san fernando valley of southern california. Bull Seismol Soc Am 111(4):2158–2166
- Boore DM, Thompson EM (2007) On using surface-source downhole-receiver logging to determine seismic slownesses. Soil Dyn Earthq Eng 27(11):971–985
- Brown LT, Boore DM, Stokoe KH (2002) Comparison of shear-wave slowness profiles at 10 strong-motion sites from noninvasive SASW measurements and measurements made in boreholes. Bull Seismol Soc Am 92(8):3116–3133
- Butcher AP, Campanella RG, Kaynia AM, Massarsch KR (2005) Seismic cone downhole procedure to measure shear wave velocity-a guideline prepared by ISSMGE TC10: Geophysical Testing in Geotechnical Engineering. In: Proceedings of the XVI international conference on soil mechanics and geotechnical engineering
- Butler DK, Curro JR (1981) Crosshole seismic testing—procedures and pitfalls. Geophysics 46(1):23–29
- Campbell KW, Boore DM (2016) Evaluation of six NEHRP B/C crustal amplification models proposed for use in Western North America. Bull Seismol Soc Am 106(2):673–686
- D7400-19 (2019) Standard test methods for downhole seismic testing. ASTM International, pp 1–11
- D7400-19 (2019) D7400/D7400M-19 standard test methods for downhole seismic testing. ASTM International, pp 1–11
- Daraei A, Sharifi F, Qader DN, Hama Ali HF, Kolivand F (2024) Prediction of the static elastic modulus of limestone using downhole seismic test in Asmari formation. Acta Geophys 72(1):247–255
- Darko AB, Molnar S, Sadrekarimi A (2020) Blind comparison of non-invasive shear wave velocity profiling with invasive methods at bridge sites in Windsor, Ontario. Soil Dyn Earthq Eng 129(October):105906
- Deere DU, Deere DW (1988) The rock quality designation (RQD) index in practice. ASTM Special Technical Publication, Philadelphia
- Di Fiore V, Albarello D, Cavuoto G, De Franco R, Pelosi N, Punzo M, Tarallo D (2020) Downhole seismic wave velocity uncertainty evaluation by theoretical simulation and experimental data



- acquired during the seismic microzonation of Central Italy. Soil Dyn Earthq Eng 138:106319
- Fernandez JA, Rix GJ, Gowdy S (2008) Inversion algorithm to evaluate velocity profiles from downhole seismic tests. In: Geotechnical earthquake engineering and soil dynamics IV, American Society of Civil Engineers, Reston, pp 1–10
- Garofalo F, Foti S, Hollender F, Bard PY, Cornou C, Cox BR, Dechamp A, Ohrnberger M, Perron V, Sicilia D, Teague D, Vergniault C (2016a) InterPACIFIC project: comparison of invasive and noninvasive methods for seismic site characterization. Part II: Intercomparison between surface-wave and borehole methods. Soil Dyn Earthq Eng 82(January):241–254
- Garofalo F, Foti S, Hollender F, Bard PY, Cornou C, Cox BR, Ohrnberger M, Sicilia D, Asten M, Di Giulio G, Forbriger T, Guillier B, Hayashi K, Martin A, Matsushima S, Mercerat D, Poggi V, Yamanaka H (2016b) InterPACIFIC project: comparison of invasive and non-invasive methods for seismic site characterization. Part I: Intra-comparison of surface wave methods. Soil Dyn Earthq Eng 82:222–240
- Hallal MM, Cox BR (2019) Theoretical evaluation of the interval method commonly used for downhole seismic testing. In: Geo-Congress 2019, American Society of Civil Engineers, Reston, pp 376–386
- Joh SH, Mok YJ (1998) Development of an inversion analysis technique for downhole seismic testing and continuous seismic CPT. J Korea Geotech Soc 14(3):95–108
- Kim D-S, Bang E-S, Kim W-C (2004a) Evaluation of various downhole data reduction methods for obtaining reliable Vs profiles. Geotech Test J 27:585–597
- Kim DS, Bang ES, Kim WC (2004b) Evaluation of various downhole data reduction methods for obtaining reliable VS profiles. Geotech Test J 27(6):585–597
- Kim DS, Park HJ, Bang ES (2013) Round Robin test for comparative study of in-situ seismic tests. In: Geotechnical and geophysical site characterization 4—proceedings of the 4th international conference on site characterization 4, ISC-4, 2, pp 1427–1434
- Kim JH, Park CB (2002) Processing of downhole S-wave seismic survey data by considering direction of polarization. J Korean Geophys Soc 5(4):321–328
- Koedel U, Karl L (2020) Determination of the damping ratio by multichannel spectral analysis of seismic downhole data. Soil Dyn Earthq Eng 136(April):106235
- Kumar A, Anbazhagan P (2023) Integration of downhole data reduction techniques for determination of Vs profiles. Geo-Congr 2023:152–161
- Kumar A, Anbazhagan P (2025) Seismic site characterization of shallow bedrock sites in peninsular India using multiple geophysical methods. Acta Geotech. https://doi.org/10.1007/ s11440-025-02534-w
- Li S (2008) Deep downhole testing: procedures and analysis for highresolution vertical seismic profiling. The University of Texas at Austin
- Michaels P (2001) Use of principal component analysis to determine down-hole tool orientation and enhance SH-waves. J Environ Eng Geophys Environ Eng Geophys Soc 6(4):175–183

- Moffat R, Correia N, Pastén C (2016) Comparison of mean shear wave velocity of the top 30 m using downhole, MASW and bender elements methods. Obras y Proyectos 20:6–15
- Mok YJ, Stokoe KH, Wilson CR (1989) Use of inverse theory to analyze downhole seismic data. In: SEG technical program expanded abstracts 1989. Society of Exploration Geophysicists, pp 23–25
- Naville C, Serbutoviez S, Throo A, Vincké O, Cecconi F (2004) Seismic While Drilling (Swd) techniques with downhole measurements, introduced by ifp and its partners in 1990–2000. Oil Gas Sci Technol 59(4):371–403
- Roblee C, Stokoe K, Fuhriman M, Nelson P (1994) Crosshole SH-wave measurements in rock and soil. In: Dynamic Geotechnical Testing II, ASTM International100 Barr Harbor Drive, PO Box C700, West Conshohocken, PA 19428-2959, pp 58–72
- Stokoe KH, Hwang S, Roberts JN, Menq FM, Keene AK, Lee RC, Redpath B (2017) Deep downhole seismic testing using a hydraulically-operated, controlled-waveform vibroseis 2. Generalized Field Arrangement for Deep Downhole Testing, pp 1–12
- Stokoe KH, Li S, Cox B, Menq F-Y, Rohay A (2008) Deep downhole seismic testing for earthquake engineering studies. In: 14th World conference on earthquake engineering: innovation, practice, safety
- Stolte AC, Cox BR (2020) Towards consideration of epistemic uncertainty in shear-wave velocity measurements obtained via seismic cone penetration testing (SCPT). Can Geotech J 57(1):48–60
- Vergniault C, Mari J-L (2020) 1 Shear velocity measurement in boreholes. In: Well seismic surveying and acoustic logging. EDP Sciences, pp 15–48
- Wang H, Wu S, Qi X, Chu J (2021a) Site characterization of reclaimed lands based on seismic cone penetration test. Eng Geol 280(November 2020):105953
- Wang H, Wu S, Qi X, Chu J (2021b) Modified refracted ray path method for determination of shear wave velocity profiles using seismic cone. Eng Geol 293(August):106330
- Wang JS, Hwang JH, Lu CC, Deng YC (2022) Measurement uncertainty of shear wave velocity: a case study of thirteen alluvium test sites in Taipei Basin. Soil Dyn Earthq Eng 155(April):107195

Publisher's Note Springer Nature remains neutral with regard to jurisdictional claims in published maps and institutional affiliations.

Springer Nature or its licensor (e.g. a society or other partner) holds exclusive rights to this article under a publishing agreement with the author(s) or other rightsholder(s); author self-archiving of the accepted manuscript version of this article is solely governed by the terms of such publishing agreement and applicable law.

